Kreusch, A. et al. Structure of the membrane channel porin from Rhodopseudomonas blastica at 2.0 Å resolution. Protein Sci. 3, 58–63

ARTICLE *in* PROTEIN SCIENCE · DECEMBER 2008

Impact Factor: 2.85 · DOI: 10.1002/pro.5560030108 · Source: PubMed

Protein Science (1994), *3*:58–63. Cambridge University Press. Printed in the USA.

Structure of the membrane channel porin from *Rhodopseudomonas blastica* at 2.0 Å resolution

A. KREUSCH,[1] A. NEUBÜSER,[1] E. SCHILTZ,[1] J. WECKESSER,[2] AND G.E. SCHULZ[1]

[1] Institut für Organische Chemie und Biochemie, Albert-Ludwigs-Universität, Albertstr. 21, D-79104 Freiburg im Breisgau, Germany
[2] Institut für Biologie II, Mikrobiologie, Albert-Ludwigs-Universität, Schänzlestr. 1, D-79104 Freiburg im Breisgau, Germany

(RECEIVED August 31, 1993; ACCEPTED October 4, 1993)

Abstract

The crystal structure of a membrane channel, homotrimeric porin from *Rhodopseudomonas blastica* has been determined at 2.0 Å resolution by multiple isomorphous replacement and structural refinement. The current model has an *R*-factor of 16.5% and consists of 289 amino acids, 238 water molecules, and 3 detergent molecules per subunit. The partial protein sequence and subsequently the complete DNA sequence were determined. The general architecture is similar to those of the structurally known porins. As a particular feature there are 3 adjacent binding sites for *n*-alkyl chains at the molecular 3-fold axis. The side chain arrangement in the channel indicates a transverse electric field across each of the 3 pore eyelets, which may explain the discrimination against nonpolar solutes. Moreover, there are 2 significantly ordered girdles of aromatic residues at the nonpolar/polar borderlines of the interface between protein and membrane. Possibly, these residues shield the polypeptide conformation against adverse membrane fluctuations.

Keywords: lipid binding site; membrane channel; porin; *Rhodopseudomonas blastica*; X-ray structure analysis

The outer membrane of gram-negative bacteria contains pore-forming proteins, porins, that allow for the passive diffusion of small polar solutes with exclusion limits around 600 Da. Porins are usually trimeric, with molecular masses between 30 and 50 kDa per subunit. They are particularly stable toward heat, detergents, and proteases (Jap & Walian, 1990; Nikaido & Saier, 1992). Structure analysis of a porin from *Rhodobacter capsulatus* showed that the diffusion pore is formed by a 16-stranded β-barrel (Weiss et al., 1990, 1991; Weiss & Schulz, 1992). The same chain fold was observed for porins OmpF and PhoE from *Escherichia coli* (Cowan et al., 1992). Here we describe the sequence and the crystal structure of a porin from the phototrophic bacterium *Rhodopseudomonas blastica*.

Results and discussion

Sequence and overall topology

The major porin from *R. blastica* is a homotrimer (Butz et al., 1993). Its sequence was derived by partial protein sequencing followed by isolation and sequencing of the porin gene. Peptide alignment to the DNA-derived sequence showed that segments 1–59, 60–82 (except Trp 72), 91–104, 109–137, 146–163, and 173–289—in total, 90% of the chain—had been identified directly. There was no difference between the DNA-derived and the chemically determined sequences. The M_r of 1 subunit was 30,597.

The major porin from *R. blastica* shows weak sequence similarities (22% identical amino acids) with the porin from *R. capsulatus*. Overall sequence homology between these 2 porins from phototrophic bacteria and other porins could not be detected (Schiltz et al., 1991). The sequence and the topology of the chain fold are given in Figure 1. Various studies showed that the bottom end of the barrel faces the periplasm and the top end faces the external medium (Bosch et al., 1989; Klebba et al., 1990; Weiss et al., 1991; Cowan et al., 1992). This orientation is confirmed by numerous charged side chains at the top end pointing to the outside and thus participating in the salt-bridge network of the lipid A and core moieties of lipopolysaccharide (LPS) and divalent cations, which integrates porin efficiently into the protective LPS layer of the outer bacterial membrane. As with the other porins (Cowan et al., 1992; Weiss & Schulz, 1992), the loops at the periplasmic end of the barrel are short, whereas those at the external end are long. The 46-residue loop between strands β5 and β6 (Fig. 1) runs into the barrel interior and forms the pore eyelet, as can be visualized in Figure 2 and Kinemage 1.

The 16 strands of the β-barrel contain 56% of all residues. All β-strands are antiparallel, and all are connected to their next

Reprint requests to: Georg E. Schulz, Institut für Organische Chemie und Biochemie, Albertstr. 21, D-79104 Freiburg im Breisgau, Germany.

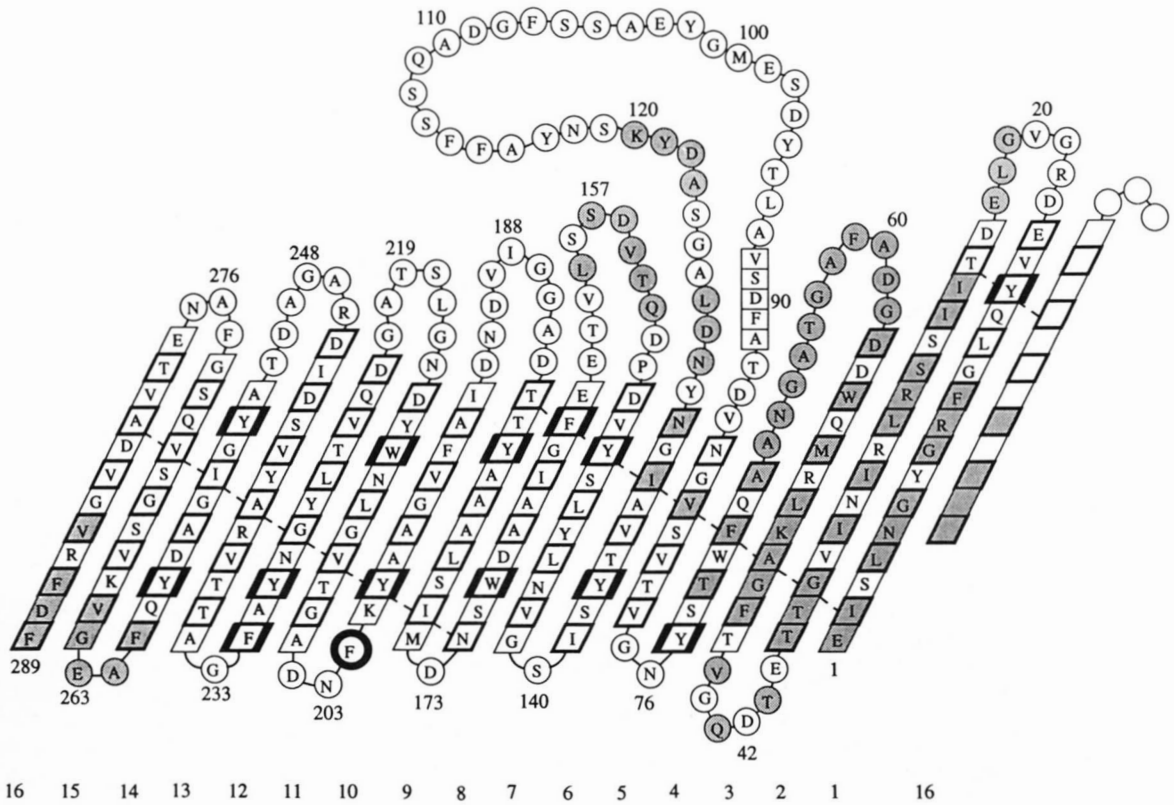

Fig. 1. Sequence and chain fold topology of porin from *R. blastica*. The view is from the outside of the 16-stranded barrel. The 71 residues involved in subunit contacts are shaded. Residues forming hydrogen bonds in the β-barrel are indicated by parallelograms (thick lines for side chains pointing to the outside, and thin lines for those pointing to the inside; aromatic residues at the nonpolar/polar borderlines are marked by particularly thick lines). The rectangles indicate an α-helix. As described in the text, the top and bottom ends of the barrel face the external medium and the periplasm, respectively. Dashed lines indicate hydrogen bonding in the β-barrel.

neighbors. The tilt angles between β-strands and the molecular 3-fold axis vary around 45°, giving rise to the normal β-sheet twist. As observed for the other known porin structures, the barrel shear number (McLachlan, 1979) is +20. A β-barrel comparison between the porins from *R. blastica* and *R. capsulatus* shows that the oval cross sections deviate markedly from each other. A superposition (Kabsch, 1978) of both β-barrels (163 C_α atoms) gives an RMS distance of 1.9 Å; it also aligns the tips of the long loops β5–β6 that constrict the pore sizes inside the barrels (average $\Delta C_\alpha = 2.3$ Å for residue positions 99–103, corresponding to 88–92 of *R. capsulatus*).

Lipid binding site

In addition to the polypeptide there emerged 3 stretches of clear density that were modeled as the detergent molecules *n*-octyltetraoxyethylene (C_8E_4) used for crystallization. Two C_8E_4 molecules bind at the nonpolar interface between protein

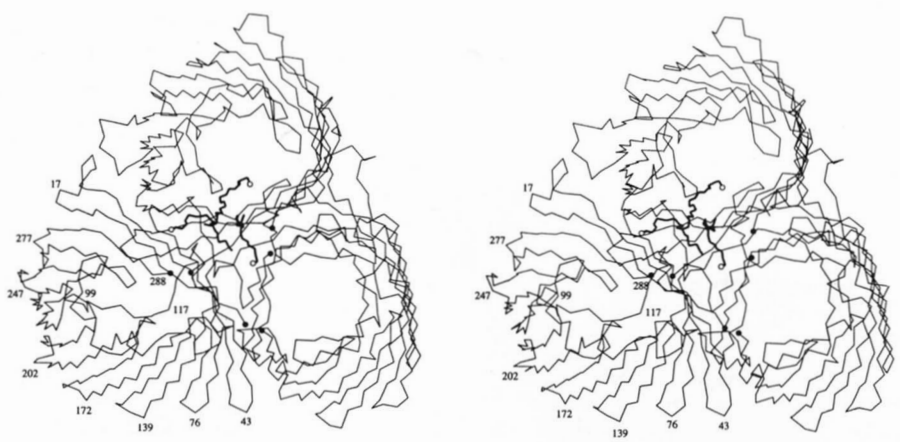

Fig. 2. Trimeric porin from *R. blastica* viewed from the external medium (top of Fig. 1) at an angle of about 30° from the molecular 3-fold axis, which is perpendicular to the membrane plane. The protein is represented by the 3 C_α backbone chain folds. The 3 symmetry-related strongly bound detergent molecules, C_8E_4, at the molecular 3-fold axis are shown as thick lines; their hydroxyl ends are marked by open circles. Some residues are numbered; the NH_2- and COOH-termini are given as dots.

and membrane. Because they have considerably higher temperature factors than the polypeptide environment (80 Å^2 vs. 20 Å^2), indicating weak binding, they are not further considered here. A strong binding site, however, was observed with the third C_8E_4 molecule per subunit at the molecular 3-fold axis, as shown in Figure 3 and Kinemage 1. This site contains density that fits 3 symmetry-related C_8E_4 molecules binding around the axis in a nonpolar pocket lined by 6 aromatic side chains, i.e., Phe 61 and Tyr 121 from each subunit. Similar binding sites involving aromatic side chains have been reported for a fatty acid binding protein (Benning et al., 1992) and for a lipid binding site in phospholipase (Van Tilbeurgh et al., 1993). The alkyl chains of the 3 symmetry-related C_8E_4 molecules have temperature factors corresponding to those of the polypeptide environment (26 Å^2 of the alkyl chain vs. 19 Å^2 for the contacting aromatic side chains), indicating strong binding.

Because this binding site is rather far away (about 20 Å) from the pore eyelets, ligand binding is not likely to hinder the permeation of solutes sterically. An allosteric effect of the ligand on the pore eyelet and thus on the channel properties is not to be expected, because binding occurs at the subunit interface moiety of the trimer, which is the most rigid part, as indicated by the crystallographic temperature factors. Obviously, this site can bind the nonpolar ends of 3 alkyl chains of an LPS molecule, which may suffice to fasten this compound although the remaining parts are dangling. This reminds us of the electron microscopy studies that suggested a bound LPS at the corresponding position of PhoE (Jap, 1989) and OmpF (Hoenger et al., 1990). No such LPS binding site, however, was found in crystals of OmpF and PhoE (Cowan et al., 1992).

Subunit interface

The height of the trimer interface at the molecular axis is about 35 Å (Fig. 2), indicating that the 3 pores are well separated over their entire lengths, which resembles the structures of the *E. coli* porins (Cowan et al., 1992). The corresponding height for the *R. capsulatus* porin is appreciably smaller (Weiss et al., 1990). The subunit interactions are extensive, involving 25% of all residues, as marked in Figure 1. The central interface moiety of the trimer contains 3 aromatic clusters, consisting of Phe 10, Phe 287, and Phe 289 from one subunit and Phe 47′ and Phe 71′ from a neighbor (Kinemage 1). The general appearance of the central interface moiety, which forms a 3-pronged star, as can be visualized in Figure 2, is that of a water-soluble protein with a nonpolar interior and a polar surface. The NH_2- and COOH-termini participate in the trimer interface, forming salt bridges with their counterparts in other subunits that fasten all chain ends. In this way, the generally weakest points of a chain fold are fixed. In contrast to the porin from *R. capsulatus* (Weiss & Schulz, 1992), the interface contains no Ca^{2+} ions and shows no sensitivity to EDTA (Butz et al., 1993).

The pore eyelet

As shown in Figure 4 and Kinemage 1, the side chains surrounding the pore eyelet are separated into a row of positive charges (mostly arginines) protruding from the barrel wall at the subunit interface side and a row of negative charges (mostly aspartates) on loop $\beta5$-$\beta6$ that runs inside the barrel forming the eyelet (Fig. 2). A similar charge separation in conjunction with 3 Ca^{2+} ions is known from the *R. capsulatus* porin (Weiss et al., 1991). At present we cannot detect any metal ions at the pore eyelet of *R. blastica*. None of the 6 sites of the Er^{3+} heavy atom derivative (see Table 1) was near the eyelet, indicating that none of the water molecules in this region had been mistaken for a Ca^{2+} ion.

Occurring in at least 2 porins, the juxtaposed rows of charges appear to be a significant feature that demands an explanation.

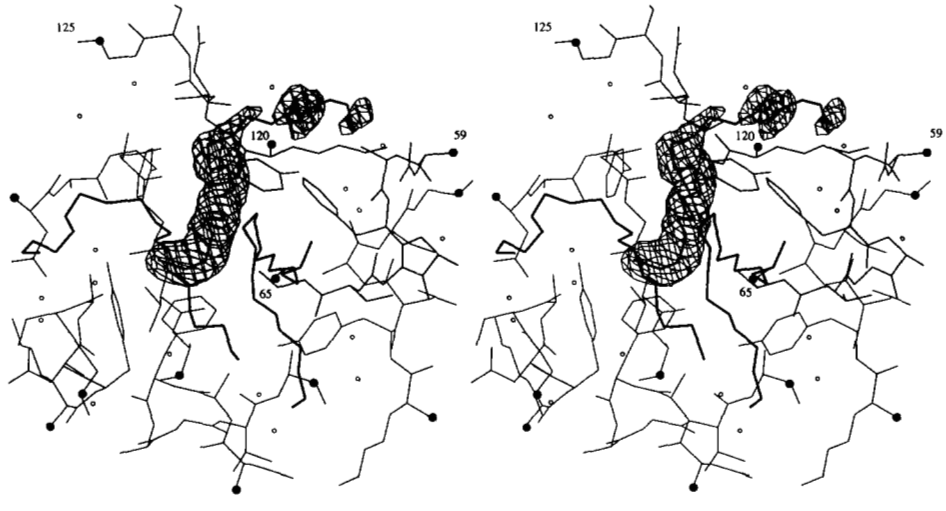

Fig. 3. Stereo view of the nonpolar, strong binding site for *n*-alkyl chains at the trimer interface superimposed by $(2F_o - F_c)$ electron density with a cut level of 1σ. The view is from the external medium approximately at an angle of 30° from the trimer axis. See Figure 2 for the general location of this site. One of the subunits has been emphasized by displaying its ligand density and by numbering. The well-defined density at the 3-fold axis has been fitted by the *n*-octyl chain and 1 oxyethylene unit of C_8E_4. The corresponding atomic temperature factors starting from the alkyl end are 23, 23, 27, 26, 29, 25, 26, 33, 44, 48, 62, and 78 Å^2. The low mobilities indicate strong binding, but there exists a gradient. There is no good density for the other 3 oxyethylene units of C_8E_4. Depicted are all residues and water molecules (◦) within about 11 Å from the trimer axis at the height of the first oxyethylene group of C_8E_4, i.e., peptide segments 59–65 and 120–125. All chain cuts are marked by dots.

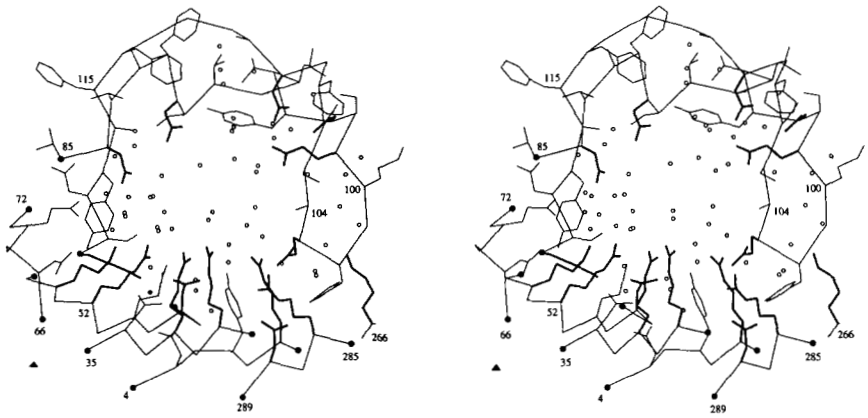

Fig. 4. Stereo view through one pore eyelet showing all side chains and water molecules (O) within about 11 Å of the pore center. For clarity, the polypeptide is merely given as the C_α backbone. The charged residues are indicated by thick lines. A separation occurs between negative charges at the upper rim of the eyelet formed by loop $\beta5$–$\beta6$ (Asp 86, Asp 90, Glu 99, Asp 109, and Asp 97 somewhat away) and positive charges at its lower rim formed by the β-barrel (Arg 9, Arg 30, Arg 32, Lys 50, Arg 52, Lys 120, Arg 286, and Lys 266 somewhat away; with compensating charges from Asp 56, Glu 103, and Asp 288). The average temperature factor of the tips of the juxtaposed positive and negative side chains is around 18 $Å^2$, indicating low mobility of the fixed charges lining the pore eyelet.

These charges should cause a transverse electric field across the pore eyelet. This field is probably rather strong, because all participating side chains are rigid (temperature factors around 18 $Å^2$) and because the charged (pH 6.8) guanidinium groups of the arginines are stacked at van der Waals distance (Fig. 4), indicating long-range electrostatic interactions.

Given this field, the pore eyelet can be considered a capacitor that stores an amount of electric energy proportional to the dielectric constant of the filling material, which is as high as 80 for water. Any intruding nonpolar solute with its much lower dielectric constant causes the stored electric energy to decrease and thus elicits a force expelling such a solute. This would explain the observed polarity separation by porins. These membrane channels are known to be easily permeable for polar solutes but discriminate against nonpolar solutes.

This suggestion is corroborated by a most simple estimate of the activation energy barrier. If the transverse electric field were caused by 5 positive and 5 negative charges placed at 2 points separated by 12 Å (in the 2 rims of the eyelet) in a homogeneous medium with a dielectric constant of 40, the electric energy loss on introducing a butane molecule (120 $Å^3$) into the center between the charges (center of eyelet) would be 12 kJ/mol. Such a barrier decelerates the permeation of butane appreciably.

The membrane-exposed surface

A prominent feature of the interface between protein and membrane is a belt of nonpolar residues along the equator of the trimer, as can be visualized in Figure 1 and more directly in Figure 5 and Kinemage 1. This belt consists mostly of middle-sized nonpolar residues, has a height of about 22 Å, corresponding to the thickness of the nonpolar moiety of the membrane (Lewis & Engelman, 1983), and is lined by aromatic residues. Aromatic residues facing the nonpolar/polar border of the membrane have also been reported for the photoreaction center (Yeates et al., 1987; Deisenhofer & Michel, 1989; Schiffer et al., 1992). The position and orientation of indole molecules at this border have been derived from thermodynamic measurements by Wimley and White (1993). In the porins, the aromatic residues form 2 prominent girdles around the trimers in which tyrosine and tryptophan side chains point with their polar groups away from the nonpolar belt, whereas the phenylalanine rings point toward the midline of the belt. This arrangement is obvious in Figure 5, and it is common for all known porin structures (Cowan et al., 1992; Weiss & Schulz, 1992) and is therefore significant.

A significant observation asks for an explanation. It is conceivable that these aromatic girdles shield the protein against ad-

Table 1. *Crystallographic data*

Data set	Resolution (Å)	Completeness (%)	Number of reflections	Number of sites	R_{merge}[a] (%)	R_{der}[b] (%)	Phasing power[c] in shells	
							100–5.5 Å	5.5–3.3 Å
Native-1	2.1	95.4	29,222	–	7.1	–	–	–
Native-2	2.0	94.7	32,882	–	5.2	–	–	–
$ErCl_3$[d]	3.0	98.4	10,185	6	4.8	15.9	2.1	1.1
$PtCl_2$	3.0	96.0	9,936	1	4.9	12.2	1.5	0.8
$FeSO_4$	3.0	85.7	8,870	1	5.1	13.3	1.75	0.4
PIP[e]	3.0	96.2	9,957	1	6.1	8.0	1.9	0.33

[a] $R_{merge} = \Sigma\Sigma|I_i - \langle I\rangle|/\Sigma\Sigma I_i$.

[b] $R_{der} = \Sigma||F_{PH}| - |F_P||/\Sigma|F_P|$; $|F_P|$ is taken from data set native-1.

[c] Ratio of RMS heavy atom structure factor amplitude divided by lack of closure error. The resulting figure of merit is 0.58 (Dickerson et al., 1968).

[d] For producing this derivative, the crystals were first soaked for 2 days in 10 mM EDTA. Then they were washed and soaked for 3 days in 10 mM $ErCl_3$.

[e] Di-μ-iodobis(ethylenediammine)-diplatinum nitrate.

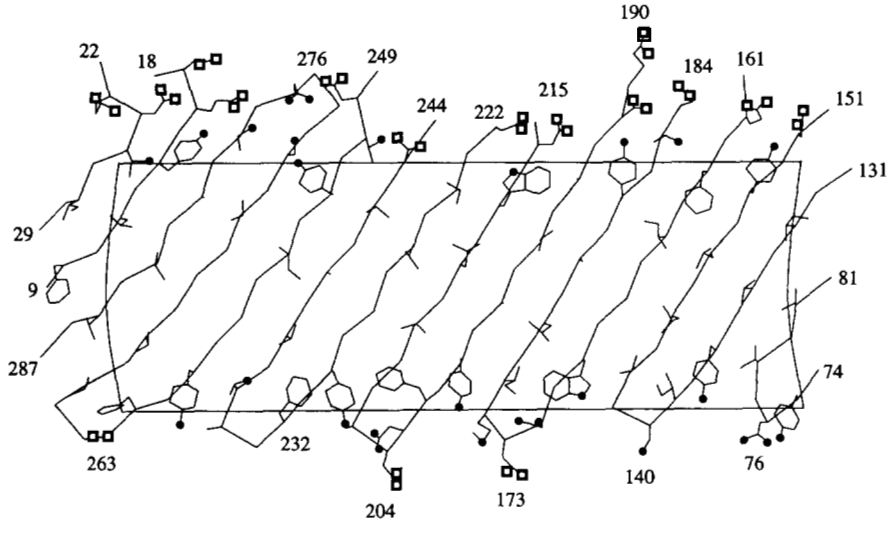

Fig. 5. Projection of the outer surface of the β-barrel onto a cylinder. Only side chains pointing to the outside are shown. Polar atoms are marked by dots and ionogenic groups by open quadrangles. The nonpolar surface exposed to the membrane is boxed; its vertical height is 22 Å. The borderlines at the left- and right-hand sides separate the membrane-exposed side chains from those buried in the subunit interface. The characteristic pattern of Phe and Tyr (Trp) residues at the outer surface is also observed in other porins.

verse membrane fluctuations. Any relative vertical displacement between membrane and protein exposes polar (nonpolar) protein surface to the nonpolar (polar) membrane moiety, causing strong surface tensions that are likely to disrupt the polypeptide conformation. In this respect, the single-layer β-sheet structure of the barrel should be particularly vulnerable. Porins may dodge such exposures by rotations of these aromatic side chains around their C_α-C_β bonds, which protrude perpendicularly from the β-sheet, i.e., the barrel surface. On vertical membrane displacement, the nonpolar phenylalanines may go along with the nonpolar (and the polar tyrosines and tryptophans along with the respective polar) moiety of the membrane and thus protect the adjacent polar (nonpolar) protein surface. Experimental data on these aromatic girdles would certainly be of great interest.

Materials and methods

Purification

The analyzed porin was isolated and purified from *R. blastica* strain DSM 2131 following a previously described protocol for *R. capsulatus* (Schiltz et al., 1991), with slight modifications: the solubilization of porin from the cell walls was done in the presence of 2% (mass/vol) *N,N*-dimethyldodecylamine-*N*-oxide (LDAO) without NaCl. The purification included an additional final gel chromatography step on a Superdex-200 prep-grade column (16 × 600 mm; Pharmacia) equilibrated with crystallization buffer.

Sequence determination

The NH_2-terminus of the protein as well as peptides isolated after cleavages with trypsin, chymotrypsin, Asp-N, and Glu-C proteases were sequenced in a pulsed-liquid gas phase sequencer (model 477A/120A, Applied Biosystems), as described by Schiltz et al. (1991) for *R. capsulatus* porin. A gene fragment was amplified by PCR using peptide-based oligonucleotides. Using this fragment as a probe, full-length genomic clones were isolated and sequenced (Neubüser, 1992). The DNA and protein sequences are deposited in the EMBL and PIR data banks.

Crystallization and structure analysis

Initially, the moderately cation-selective porin from *R. blastica* yielded crystals that diffracted to 3.2 Å resolution (Butz et al., 1993). After modifying purification and crystallization protocols, we routinely obtained crystals diffracting to beyond 2.0 Å resolution (Schulz et al., 1992). Porin was crystallized using the hanging drop method at 20 °C. The drop contained 5 mg/mL protein, 20 mM Tris/HCl at pH 6.8, 0.3–0.4 M LiCl, 0.6% *n*-octyltetraoxyethylene (C_8E_4), and 12–18% polyethylene glycol-600 (PEG-600). The reservoir was 30–38% PEG-600. Crystals grew within 2–6 weeks. The space group is R3 ($a = b = 104.3$ Å, $c = 125.1$ Å) with 1 subunit per crystallographic asymmetric unit. All X-ray data were collected on an area detector (model X1000, Xentronics/Siemens) and processed with the program XDS (Kabsch, 1988).

The structure could not be solved by molecular replacement based on the weakly related porin from *R. capsulatus*. We therefore applied the multiple isomorphous replacement (m.i.r.) method. Initial phases were obtained by solving the difference-Patterson map of the heavy atom derivative produced with $ErCl_3$. Interpretation of the other derivatives followed (Table 1). All heavy atom parameters were refined (Dickerson et al., 1968), showing that the most important phase contributions came from the Er^{3+} derivative, which in addition indicated possible Ca^{2+} sites (Blundell & Johnson, 1976). The m.i.r. phases were improved by solvent-flattening (Wang, 1985), yielding an interpretable electron density map at 3.3 Å resolution.

Model building into this map and manual interventions were done within the program O (Jones et al., 1991). The model was refined using the program suite XPLOR (Brünger et al., 1987). The current *R*-factor is 16.5% for all reflections in the resolution range from 10 to 2.0 Å at reasonable model geometry; the RMS deviations from ideal geometry are 0.016 Å for bond lengths and 2.9° for bond angles. Coordinates are deposited with the Protein Data Bank (Brookhaven, New York).

References

Benning MM, Smith AF, Wells MA, Holden HM. 1992. Crystallization, structure determination and least-squares refinement to 1.75 Å of the fatty-acid-binding protein isolated from *Manduca sexta* L. *J Mol Biol 228*:208–219.

Blundell TL, Johnson LN. 1976. *Protein Crystallography*. London: Academic Press. pp 184–188.

Bosch D, Scholten M, Verhagen C, Tommassen J. 1989. The role of the carboxy-terminal membrane-spanning fragment in the biogenesis of *Escherichia coli* K12 outer membrane protein PhoE. *Mol Gen Genet 216*:144–148.

Brünger AT, Kuriyan J, Karplus M. 1987. Crystallographic *R*-factor refinement by molecular dynamics. *Science 235*:458–460.

Butz S, Benz R, Wacker T, Welte W, Lustig A, Plapp R, Weckesser J. 1993. Biochemical characterization and crystallization of porin from *Rhodopseudomonas blastica*. *Arch Microbiol 159*:301–307.

Cowan SW, Schirmer T, Rummel G, Steiert M, Ghosh R, Pauptit RA, Jansonius JN, Rosenbusch JP. 1992. Crystal structures explain functional properties of two *E. coli* porins. *Nature 358*:727–733.

Deisenhofer J, Michel H. 1989. The photosynthetic reaction center from the purple bacterium *Rhodopseudomonas viridis*. *Science 245*:1463–1473.

Dickerson RE, Weinzierl JE, Palmer RA. 1968. A least squares refinement method for isomorphous replacement. *Acta Crystallogr B 24*:997–1003.

Hoenger A, Gross H, Aebi U, Engel A. 1990. Localization of the lipopolysaccharides in metal-shadowed reconstituted lipid-porin membranes. *J Struct Biol 103*:185–195.

Jap BK. 1989. Molecular design of PhoE porin and its functional consequences. *J Mol Biol 205*:407–419.

Jap BK, Walian PJ. 1990. Biophysics of the structure and function of porins. *Q Rev Biophys 23*:367–403.

Jones TA, Zou JY, Cowan SW, Kjeldgaard M. 1991. Improved methods for building protein models in electron density maps and the location of errors in these models. *Acta Crystallogr A 47*:110–119.

Kabsch W. 1978. A discussion of the solution for the best rotation to relate two sets of vectors. *Acta Crystallogr A 34*:827–830.

Kabsch W. 1988. Evaluation of single crystal X-ray diffraction from a position-sensitive detector. *J Appl Crystallogr 21*:916–924.

Klebba PE, Benson SA, Bala S, Abdullah T, Reid J, Singh SP, Nikaido H. 1990. Determinants of OmpF porin antigenicity and structure. *J Biol Chem 265*:6800–6810.

Lewis BA, Engelman DM. 1983. Bacteriorhodopsin remains dispersed in fluid phospholipid bilayers over a wide range of bilayer thickness. *J Mol Biol 166*:211–217.

McLachlan AD. 1979. Gene duplication in the structure evolution of chymotrypsin. *J Mol Biol 128*:49–79.

Neubüser A. 1992. Klonierung und Sequenzierung des Poringens aus *Rhodopseudomonas blastica* [thesis]. Freiburg im Breisgau, Germany: Albert-Ludwigs-Universität.

Nikaido H, Saier MH Jr. 1992. Transport proteins in bacteria: Common themes in their design. *Science 258*:936–942.

Schiffer M, Chang CH, Stevens FJ. 1992. The functions of tryptophan residues in membrane proteins. *Protein Eng 5*:213–214.

Schiltz E, Kreusch A, Nestel U, Schulz GE. 1991. Primary structure of porin from *Rhodobacter capsulatus*. *Eur J Biochem 199*:587–594.

Schulz GE, Dreyer M, Klein C, Kreusch A, Mittl P, Müller CW, Müller-Dieckmann J, Muller Y, Proba K, Schlauderer G, Spürgin P, Stehle T, Weiss MS. 1992. Highly ordered crystals of channel-forming membrane proteins, of nucleoside-monophosphate kinases, of FAD-containing oxidoreductases and of sugar-processing enzymes and their mutants. *J Crystal Growth 122*:385–392.

Van Tilbeurgh H, Egloff MP, Martinez C, Rugani N, Verger R, Cambillau C. 1993. Interfacial activation of the lipase–procolipase complex by mixed micelles revealed by X-ray crystallography. *Nature 362*:814–820.

Wang BC. 1985. Resolution of phase ambiguity in macromolecular crystallography. *Methods Enzymol 115*:90–112.

Weiss MS, Abele U, Weckesser J, Welte W, Schiltz E, Schulz GE. 1991. Molecular architecture and electrostatic properties of a bacterial porin. *Science 254*:1627–1630.

Weiss MS, Schulz GE. 1992. Structure of porin refined at 1.8 Å resolution. *J Mol Biol 227*:493–509.

Weiss MS, Wacker T, Weckesser J, Welte W, Schulz GE. 1990. Three dimensional structure of porin from *Rhodobacter capsulatus* at 3 Å resolution. *FEBS Lett 267*:268–272.

Wimley WC, White SH. 1993. Membrane partitioning: Distinguishing bilayer effects from the hydrophobic effect. *Biochemistry 32*:6307–6312.

Yeates TO, Komiya H, Rees DC, Allen JP, Feher G. 1987. Structure of the reaction center from *Rhodobacter sphaeroides* R-26: Membrane-protein interactions. *Proc Natl Acad Sci USA 84*:6438–6442.